

Azanitrile Inhibitors of the SmCB1 Protease Target Are Lethal to *Schistosoma mansoni*: Structural and Mechanistic Insights into Chemotype Reactivity

Adéla Jílková,[‡] Martin Horn,[‡] Jindřich Fanfrlík, Jim Küppers, Petr Pachl, Pavlína Řezáčová, Martin Lepšík, Pavla Fajtová, Petra Rubešová, Marta Chanová, Conor R. Caffrey, Michael Gütschow,* and Michael Mareš*



Cite This: *ACS Infect. Dis.* 2021, 7, 189–201



Read Online

ACCESS |



Metrics & More



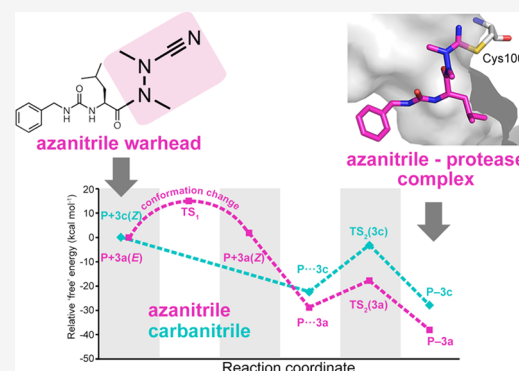
Article Recommendations



Supporting Information

ABSTRACT: Azapeptide nitriles are postulated to reversibly covalently react with the active-site cysteine residue of cysteine proteases and form isothiosemicarbazide adducts. We investigated the interaction of azadipeptide nitriles with the cathepsin B1 drug target (SmCB1) from *Schistosoma mansoni*, a pathogen that causes the global neglected disease schistosomiasis. Azadipeptide nitriles were superior inhibitors of SmCB1 over their parent carba analogs. We determined the crystal structure of SmCB1 in complex with an azadipeptide nitrile and analyzed the reaction mechanism using quantum chemical calculations. The data demonstrate that azadipeptide nitriles, in contrast to their carba counterparts, undergo a change from *E*- to *Z*-configuration upon binding, which gives rise to a highly favorable energy profile of noncovalent and covalent complex formation. Finally, azadipeptide nitriles were considerably more lethal than their carba analogs against the schistosome pathogen in culture, supporting the further development of this chemotype as a treatment for schistosomiasis.

KEYWORDS: azapeptide inhibitors, cysteine proteases, protein structures, structure–activity relationships, schistosomiasis



Azapeptides, peptides in which the $\text{C}\alpha\text{H}$ of at least one amino acid has been replaced with nitrogen, have emerged as particularly important peptidomimetic structures (Figure 1). Compared to their parent carbapeptide analogs, bioactive azapeptides can possess improved potency and target selectivity as well as superior pharmacokinetics.^{1–5} Azadipeptide nitriles were introduced as a class of efficient inhibitors of human cysteine cathepsins.^{6–9} This chemotype supported the successful development of activity-based probes, modified for organelle-specific delivery to lysosomal cysteine proteases and applied as PET-imaging agents for tumor-associated cathepsin activity.^{10–12} These reports have highlighted that azadipeptide nitriles can enrich the portfolio of inhibitors of cysteine proteases suitable as activity-based probes^{13,14} and potential therapeutics against parasitic and protozoal infections.^{15–18} Similar to the well-established dipeptide nitriles, azadipeptide nitriles are thought to undergo a covalent, reversible interaction with the target proteases by forming a stabilized isothiosemicarbazide adduct (Figure 1).^{6–12}

Here, we investigated the interaction of aza- and carbadipeptide nitriles with cathepsin B1 (SmCB1) from the human blood fluke, *Schistosoma mansoni*.^{19,20} Trematode flatworms of the genus *Schistosoma* cause schistosomiasis

(bilharzia), a chronic disease that infects over 200 million people in tropical and subtropical areas.²¹ As treatment and control of schistosomiasis rely on just one drug, praziquantel, there is impetus to identify new antischistosomal.^{22–25} The cysteine protease SmCB1 is a central digestive enzyme of the parasite and has been validated as a chemotherapeutic target for the cure of schistosomiasis.^{20,26} Previously, we determined the crystal structure of SmCB1 as a footing for rational drug development.^{20,27,28}

In this study, we compared the functional properties of dipeptides with azanitrile and carbanitrile warheads and found azanitriles to be superior. The azadipeptide nitriles were potent inhibitors of SmCB1 with antischistosomal activity and, thus, represent a new class of potential drug leads. We present the first crystallographic analysis of a protease–azanitrile inhibitor complex and quantum chemical calculations to provide

Received: September 10, 2020

Published: December 10, 2020



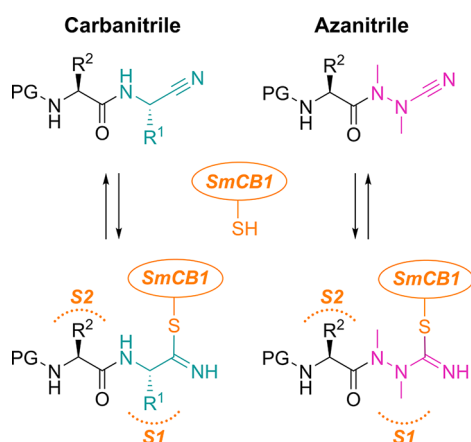


Figure 1. Carba- and azadipeptide nitriles and their reaction with cysteine proteases. Isoelectronic CαH/N exchange in the warhead (cyan/magenta) of dipeptide nitriles (left) leads to azadipeptide nitriles (right). Two carbohydrazide nitrogens in azanitriles need to be alkylated to circumvent spontaneous heterocyclization.⁶ R¹ and R² are substituents in amino acid residues at the P1 and P2 positions (binding in the enzyme subsites S1 and S2), respectively; PG is a protecting group. The depicted azadipeptide bears an aza-alanine nitrile at the P1 position. Reactive warheads of both chemotypes form a covalent, reversible bond with the thiol of the catalytic cysteine residue (orange) of papain-family cysteine proteases (represented by SmCB1).

mechanistic insight into the phenomenon of azanitrile warhead reactivity.

RESULTS AND DISCUSSION

SAR Analysis of Aza- and Carbadipeptide Nitriles Reveals a High Potency of SmCB1 Inhibitors with an Azanitrile Warhead. We have evaluated a set of 18 azadipeptide and 50 carbadipeptide nitriles *in vitro* as potential inhibitors of the SmCB1 protease. The compound scaffold is defined by positions P3 through P1 (Schechter and Berger nomenclature),²⁹ and the substitutions were selected to provide a high diversity in all positions. The compounds were screened against recombinant SmCB1, and their K_i values were determined using a kinetic inhibition assay with the fluorogenic substrate Cbz-Phe-Arg-AMC. The data for seven representative pairs of both chemotypes are shown in Table 1. Analogs with the azanitrile warhead (1a–7a) were more potent than those with the carbanitrile warhead (1c–7c). This general trend was confirmed for the entire set of test compounds (Tables S1 and S2). Most of the aza compounds were effective in nanomolar concentrations with slow-binding kinetics, whereas only 10% of the carba compounds had K_i values <1 μM and had fast-binding behavior with linear progress curves (Figure 2), a typical feature of peptidic (carba)nitrile inhibitors of cysteine proteases.^{9,30,31} Using the example of the Cbz-capped phenylalanine pair (2a and 2c), additional variations in the carbanitrile warhead by the stepwise introduction of methyl groups at the amino-acetonitrile unit (i.e., the incorporation of alanine, sarcosine, or *N*-methylalanine-derived nitrile building blocks in 8c–10c) did not improve the inhibition of SmCB1 (Table 2).

Table 3 shows the SAR analysis of the P1 to P3 positions of the azanitrile scaffold. The presence of the azanitrile warhead was not sufficient for strong potency, as compound 1a, which lacks a residue side chain for the P2–S2 interaction, was not

Table 1. Pairs of Peptidomimetics with Aza- or Carbanitrile Warheads and Their Inhibition Potency against SmCB1

Peptidomimetic core	SmCB1 inhibition K _i (nM) ^a (Cpd)	
	Warhead R	
	31 100 ± 1500 (1a)	>100 000 (1c)
	19.4 ± 1.4 (2a)	2920 ± 320 (2c)
	6.1 ± 0.7 (3a)	>100 000 (3c)
	36.7 ± 2.6 (4a)	6620 ± 910 (4c)
	4.8 ± 0.3 (5a)	1215 ± 205 (5c)
	1540 ± 250 (6a)	>100 000 (6c)
	229 ± 7 (7a)	>100 000 (7c)

^aThe K_i values were determined using a kinetic activity assay with the fluorogenic peptide substrate Cbz-Phe-Arg-AMC.

active. Larger hydrophobic and aromatic residues at the P2 position strengthen binding to the protease (1a versus 2a, 11a). Also, modification of the α-nitrogen substituent in the aza-amino nitrile unit of 2a by extended hydrophobic P1 substituents could improve inhibition (2a versus 8a, 9a). In the P3 position, the introduction of a benzyl urea moiety as present in 3a markedly increased the inhibitory potency. A comparison of P3 triaryl compounds, each with leucine in the P2 position (4a, 5a, 17a), showed that the amide linkage and the associated triaryl group (5a) was preferred over the urea and methylurea linkages (4a and 17a, respectively). The amide bond contributes to the binding affinity because its methylation decreased potency 300-fold (5a versus 6a). When the entire structure of 5a was maintained but leucine was replaced with a less appropriate P2 amino acid, i.e., homocycloleucine in 7a, a 40-fold decrease in potency was measured. Also, we analyzed the second-order rate constants of azadipeptide nitriles (k_{2nd}, Table S1). The k_{2nd} values of the five most potent compounds with single-digit nM K_i values (from 4.6 to 6.2 nM) were particularly high for 3a, 5a, and 11a

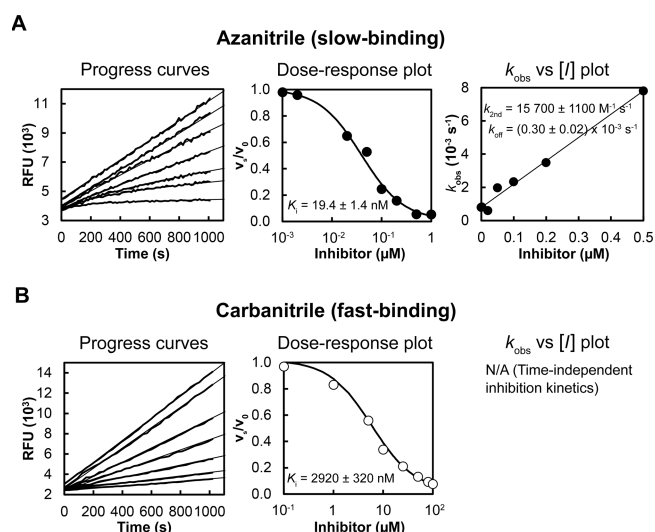


Figure 2. Different binding kinetics of SmCB1 inhibitors with azanitrile and carbanitrile warheads represented by **2a** and **2c**, respectively. Progress curves show the hydrolysis of the fluorogenic substrate Cbz-Phe-Arg-AMC by SmCB1 in the presence of increasing inhibitor concentrations. (A) The azanitrile exhibited a time-dependent inhibition characterized by nonlinear progress curves typical of slow-binding kinetics. (B) Linear progress curves obtained for the carbanitrile are characteristic of fast-binding inhibitors. In dose–response plots, the derived steady-state reaction velocities were plotted against inhibitor concentration, and the inhibition constants K_i were obtained. In the k_{obs} versus $[I]$ plot, the first-order rate constants k_{obs} from the time-dependent progress curves were plotted against inhibitor concentrations to show a linear dependence. For details on data fitting and kinetic parameters, see the [Methods](#).

Table 2. Effect of Variations in the Carbanitrile Warhead on SmCB1 Inhibition

Compound	Warhead R	SmCB1 inhibition ^a K_i (nM)
2a		19.4 ± 1.4
2c		2920 ± 320
8c		11 000 ± 1600
9c		>100 000
10c		>100 000

^aThe K_i values were determined using a kinetic activity assay with the fluorogenic peptide substrate Cbz-Phe-Arg-AMC.

(20.4, 29.0, and $32.7 \times 10^3 \text{ M}^{-1} \text{ s}^{-1}$, respectively) and somewhat lower for **8a** and **9a** (5.2 and $2.1 \times 10^3 \text{ M}^{-1} \text{ s}^{-1}$), indicating a slower association of the enzyme–inhibitor complex, presumably due to the presence of the large P1

substituents in **8a** and **9a** ($R_1 = \text{Bn-CH}_2-$ and $\text{CH}_3-(\text{CH}_2)_4-$, respectively).

Phenotypic Effects of Azanitriles on *Schistosoma mansoni*. A panel of 35 azanitrile and carbanitrile inhibitors that were effective against SmCB1 (Tables 1–3 and S2) was phenotypically screened *in vitro* at $10 \mu\text{M}$ against *S. mansoni* newly transformed schistosomula (NTS), the postinvasive stage of the parasite that feeds on host blood. The resulting phenotypic responses were graded from 0 through 4, i.e., from the least to the most severe. Figure 3 compares the severity scores for the azanitrile and carbanitrile analog pairs (for complete phenotyping data for the panel, see Table S3). We found that both inhibitor chemotypes substantially differed in their bioactivities.

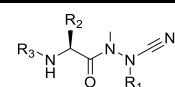
The azanitrile inhibitors caused rapid and severe phenotypes (scores of 3 and 4) except for **1a**, which was ineffective against NTS and SmCB1. In contrast, the incubation of NTS with the carbanitrile analogs resulted in more occasional and lower severity scores. The correlation between the severity scores generated by the azanitriles against the parasite and their potency of inhibition of SmCB1 was highly significant (Table S3, Spearman correlation test with nonzero value coefficients, 20 000 permutations, $p < 0.001$). The most inhibitory azanitriles (with K_i values in the single-digit nM range) were also tested for their cytotoxicity against two human cell lines. They displayed low cytotoxicity at the same concentrations used in the NTS assay (Table S4), indicating that the observed phenotypic changes were specific to the parasite. In conclusion, azadipeptide nitriles that target SmCB1 were demonstrated to be effective antischistosomal compounds.

Crystallographic Analysis Identifies the Binding Mode of Azanitriles to SmCB1. The crystal structure of SmCB1 in complex with the single-digit nanomolar inhibitor **3a** was determined at a resolution of 1.3 Å (PDB ID: 6YI7; Table S5). The binding mode of **3a** in the active site is presented in Figure 4. The inhibitor's P1 to P3 residues occupy the S1 to S3 binding subsites of SmCB1. Through the nucleophilic attack of the thiol group of the catalytic Cys100 residue, an isothiosemicarbazide adduct is formed that incorporates the C_{AB} atom of the nitrile moiety (Figures 4D and S1). The N_{AA} atom of the nitrile moiety is stabilized by two hydrogen bonds to the backbone amide of Cys100 and the side chain amide of Gln94 (Figure 4D). Analogous interactions were observed in the structure of rat cathepsin B complexed with a carbanitrile inhibitor.³²

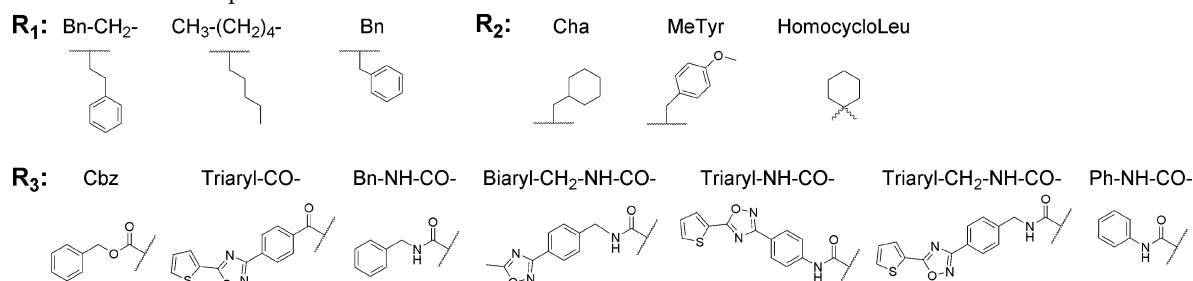
Azadipeptides are atropochiral molecules due to the restricted rotation around the methylated N–N axis. The induction of chirality was demonstrated by methylation of the hydrazine fragment in model azapeptides, which led to the *E*-configuration of the respective CO–N bond and, hence, to atropisomerism.³³ However, *E*-configured peptidomimetic ligands should possess a weaker affinity for the active site of a protease than the *Z*-configured isomers. This is also supported by data for cathepsin inhibition involving *E*- and *Z*-locked azadipeptide nitriles.³⁴ The configuration of non-locked azadipeptide nitriles bound to the protease active site is so far unknown. Noteworthy, in this study, we were able to demonstrate the *Z*-configuration of the $C(\text{O})-N_{AE}(N_{AC})$ fragment for the enzyme-bound prototypical inhibitor **3a** (Figure 4).

Insights were also gained into the binding with the S2 and S3 subsites. At the P2 position, **3a** contains a leucine substituent making nonpolar interactions with residues

Table 3. Inhibition of SmCB1 and Antischistosomal Activity of Azadipeptide Nitriles

Compound ^a	Substituent position ^b			SmCB1 inhibition ^c <i>K_i</i> (nM)	Antischistosomal effect ^d Day 1/ Day 2 (Severity score)
	R ₃	R ₂	R ₁		
					
P1 substitution					
2a ^e	Cbz	Phe	CH ₃ -	19.4 ± 1.4	4/4
8a	Cbz	Phe	Bn-CH ₂ -	4.8 ± 0.2	4/4
9a	Cbz	Phe	CH ₃ -(CH ₂) ₄ -	6.2 ± 0.5	4/4
10a	Cbz	Phe	Bn-	48.9 ± 4.7	2/4
P2 substitution					
1a	Cbz	Gly	CH ₃ -	31 100 ± 1500	0/0
2a ^e	Cbz	Phe	CH ₃ -	19.4 ± 1.4	4/4
11a	Cbz	Cha	CH ₃ -	4.6 ± 0.5	2/4
12a	Cbz	Ile	CH ₃ -	71.7 ± 4.4	4/4
13a	Cbz	MeTyr	CH ₃ -	80.6 ± 7.1	4/4
14a	Cbz	Val	CH ₃ -	88.3 ± 10.4	3/4
15a	Cbz	Ala	CH ₃ -	714 ± 58	2/4
P3 substitution					
3a	Bn-NH-CO-	Leu	CH ₃ -	6.1 ± 0.7	3/4
4a	Triaryl-NH-CO-	Leu	CH ₃ -	36.7 ± 2.6	3/4
5a	Triaryl-CO-	Leu	CH ₃ -	4.8 ± 0.3	2/4
6a	Triaryl-CO-	Leu ^f	CH ₃ -	1540 ± 250	4/4
7a	Triaryl-CO-	HomocycloLeu	CH ₃ -	229 ± 7	3/4
16a	Biaryl-CH ₂ -NH-CO-	Leu	CH ₃ -	30.0 ± 4.1	0/2
17a	Triaryl-CH ₂ -NH-CO-	Leu	CH ₃ -	58.3 ± 2.8	0/0
18a	Ph-NH-CO-	Leu	CH ₃ -	112 ± 11	2/4

^aCompounds 1a to 7a are also presented in Table 1. ^bThe abbreviations used are as follows:



^cThe *K_i* values were determined using a kinetic activity assay with the fluorogenic peptide substrate Cbz-Phe-Arg-AMC. ^dPhenotypic changes in the parasite in the presence of 10 μM inhibitor are indicated for 24 and 48 h (see Table S3) and converted to a severity score on a scale from 0 (no effect) to 4 (severe). ^e2a is listed in both P1 and P2 sections. ^fN-Methylated leucine.

Ala271 and Leu146 of SmCB1 (Figure 4C). Residue Glu316 in the S2 subsite has been shown to rotate out of the binding pocket to avoid steric clash with bulky ligand substituents.²⁰ In the SmCB1–3a complex, the flexibility of Glu316 was demonstrated by its dual conformation with one of the conformations making contact with the P2 leucine. The P3 position of the inhibitor is formed by a benzylaminocarbonyl group. The lower value of the electron density of this substituent suggests its static or dynamic disorder (Figure S2). In the crystallographic model, one conformation of the benzylaminocarbonyl moiety was modeled into the electron density map, representing the major position. Nevertheless, it is obvious that the P3 substituent can acquire several alternative positions within the S3 subsite, which is rather wide and less engaged in ligand binding.²⁰

Quantum Chemical Calculations Demonstrate the Highly Favorable Energetics of the Azanitrile Reaction Mechanism. Computational approaches based on quantum mechanics have proven powerful in exploring catalytic mechanisms of cysteine proteases and designing their covalent inhibitors.^{20,35–39} In the present study, quantum chemical calculations were employed to analyze the “free” energy profile of the binding reaction of 3a to SmCB1, proceeding via a noncovalent intermediate to the final covalent complex (Figure 5A; “free” energies refer to the sums of gas phase energies and solvation free energies). We observed different configurations of the planar amide group C(O)–N(N) at the warhead (Figure 5B). The bound 3a adopts the *Z*-configuration as seen in the SmCB1–3a crystallographic complex; however, the modeling of unbound 3a reveals that the *E*-configuration is more stable in solvent (by 1.9 kcal mol^{−1}) (Table S6 and

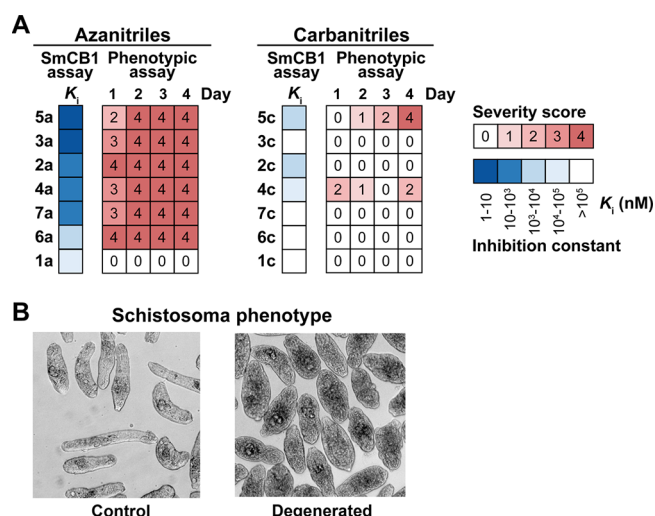


Figure 3. Correlation of the antischistosomal activity with the inhibition of SmCB1 by azanitrile and carbanitrile analogs. (A) Pairs of analogs with azanitrile and carbanitrile warheads were phenotypically screened against *S. mansoni* newly transformed schistosomula (NTS) and the data arising was compared to those for the inhibition of SmCB1. Phenotypic changes in the parasite (Table S3) were observed every day for 4 days in the presence of 10 μ M inhibitor. Changes were converted to a severity score on a scale from 0 (no effect) to 4 (severe; red heat map). K_i values for SmCB1 inhibition (from Table 1) are shown in the blue heat map. (B) An example of an inhibitor-induced degenerated phenotype in NTS of *S. mansoni* versus untreated controls (for details, see Table S3).

Figure S3). This is in line with the preferred *E*-conformation determined experimentally for other free azanitriles and trisubstituted hydrazides in general.^{33,34,40,41} Thus, 3a under-

goes a conformational change upon binding to the enzyme. The activation energy for the *E*- to *Z*-conversion calculated using the implicit solvent model was approximately 15 kcal mol⁻¹ (Table S6). This rotational barrier is a possible explanation for the slow binding of azanitriles to SmCB1 observed in the inhibition kinetics (Figure 2). On the contrary, for the carbanitrile, 3c, the *Z*-configuration of the C(O)–N(C) moiety was more stable than the *E*-configuration for both the modeled SmCB1–3c complex and the uncomplexed 3c (by 3.1 and 2.0 kcal mol⁻¹, respectively) (Figure S3 and the Supplementary Results). This agrees with the *Z*-configuration reported for various protease-bound and free carbanitriles.^{32,33} The fact that no conformational change is required for the interaction of 3c with the enzyme determines the fast-binding kinetics of carbanitriles to SmCB1 (Figure 2).

We next investigated the intermediate noncovalent complexes of 3a and 3c with SmCB1. In optimized noncovalent models, the catalytic residue His270 is positively charged, and the thiolate sulfur atom of Cys100 is separated by about 3.2 Å from the C_{AB} atom of the inhibitor (Figure 5C). The formation of the noncovalent complex is energetically favorable for both inhibitors with a higher “free” energy gain for 3a (Figure 5A, Table S6). The stronger noncovalent interaction of 3a might be the result of a distinct electrostatic pattern of the azanitrile warhead (Figure S4 and the Supplementary Results). Conversion to the covalent complex is associated with the formation of a covalent bond between the S atom of Cys100 and C_{AB} atom of the inhibitor and a concomitant water-mediated proton transfer from His270 to the N_{AA} atom of the nitrile group (Figure 5C). The transformation proceeds via a transition state with the S...C_{AB} distance of about 2.3 Å and a proton localized on H₃O⁺ (crystallographic water molecule 628). The transition barrier is 11.1 and 19.2 kcal mol⁻¹ for 3a

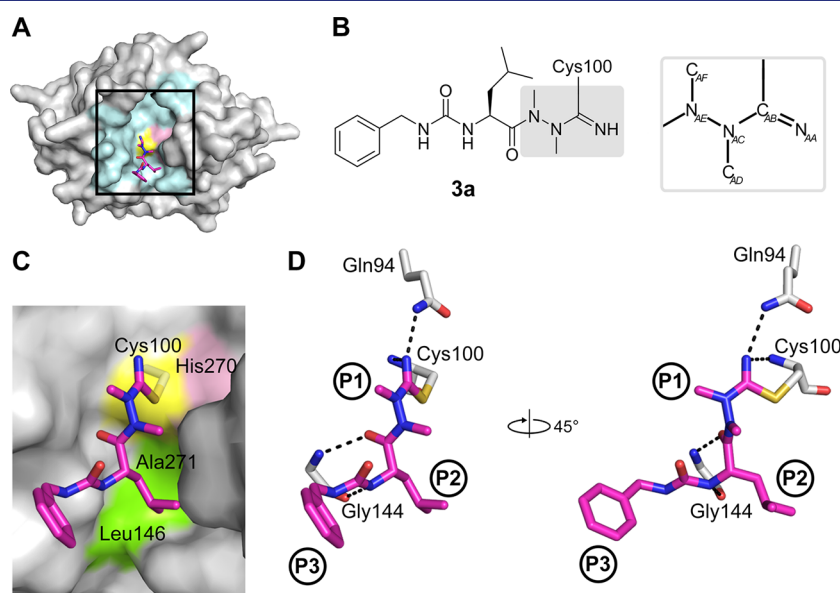


Figure 4. Binding mode of the azadipeptide nitrile inhibitor 3a in the SmCB1 active site. (A) Overall crystal structure of the SmCB1–3a complex in surface (enzyme) and stick (inhibitor) representation. In the SmCB1 active site (boxed), the catalytic residues Cys100 (yellow) and His270 (pink) and major subsite residues (cyan) are highlighted. (B) Chemical structure of 3a forming a covalent bond with the S atom of the catalytic Cys100. The azanitrile warhead is boxed in gray, and atom labeling is indicated (hydrogen atoms are omitted). (C) Zoomed view of (A) showing the active site residues that form nonpolar interactions (green) with 3a (in stick representation with carbon atoms in magenta); the catalytic residues are also indicated. (D) The P1 to P3 positions of the inhibitor bind the corresponding S1 to S3 subsites of the SmCB1 active site. Dashed lines indicate hydrogen bonds formed between SmCB1 residues (gray) and 3a (magenta); heteroatoms have standard color coding (O, red; N, blue; S, yellow). Coordinates are deposited under PDB code 6YI7.

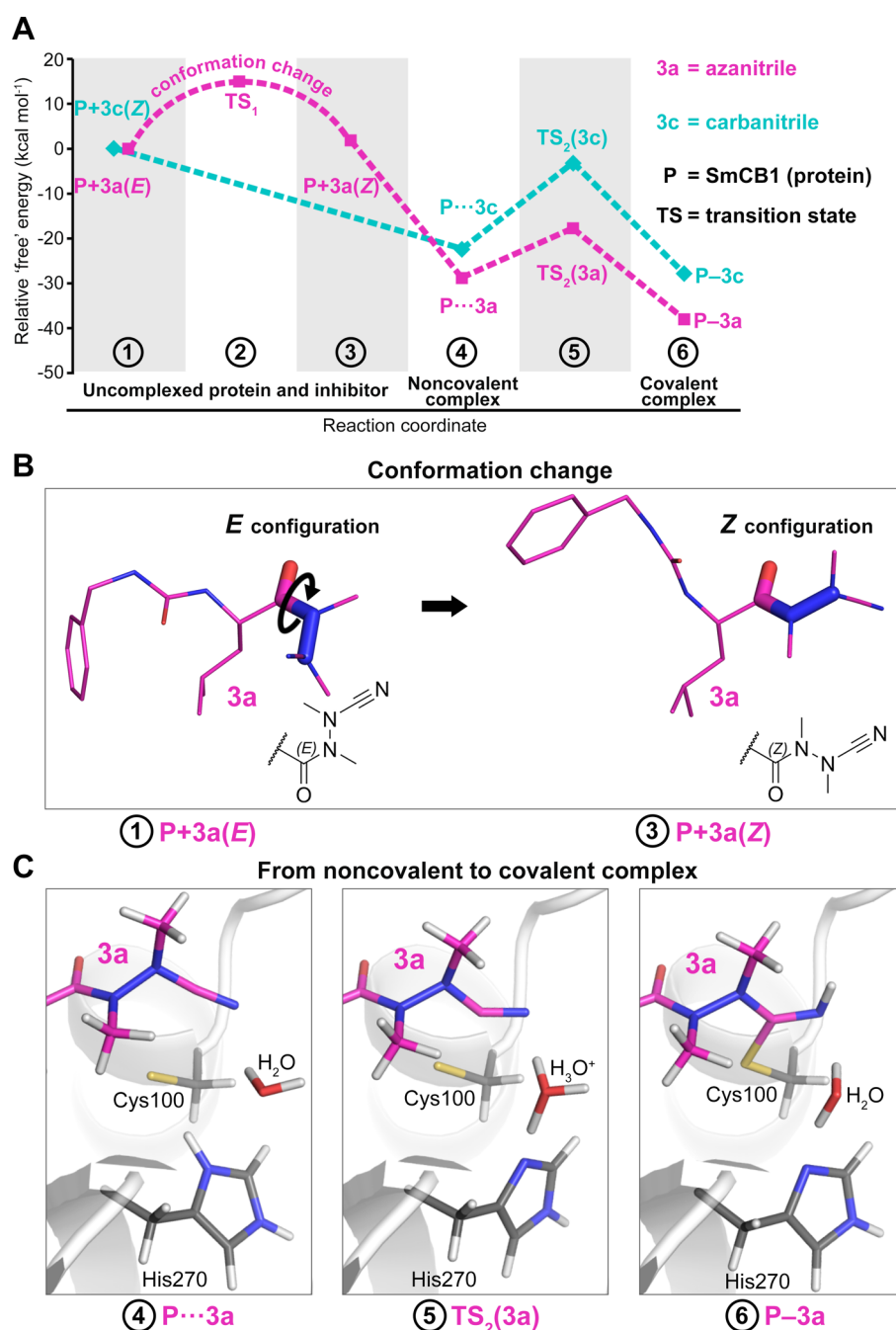
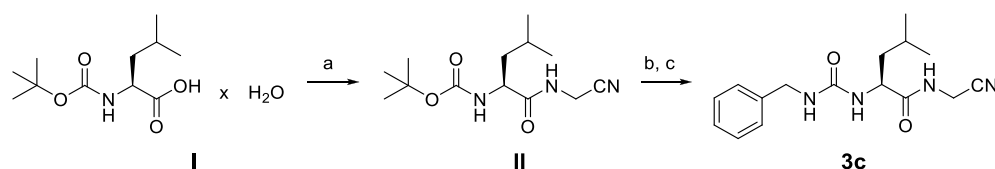


Figure 5. Computational analysis of the binding reaction of azanitrile and carbanitrile inhibitors to the active site of SmCB1. (A) The “free” energy profile of the binding of azanitrile 3a and carbanitrile 3c was determined using quantum chemical calculations. Individual states along the reaction pathway (indicated by numbers) are defined by their relative “free” energies (Table S6). (B) The unbound azanitrile inhibitor has the *E*-configuration in solution (with minimum “free” energy) and undergoes a conformational change to the *Z*-configuration that was also demonstrated crystallographically in the SmCB1–3a complex. (C) Modeled states upon binding of the azanitrile inhibitor to the active site include an initial noncovalent complex (4), a transition state with proton transfer from His270 to H₂O (5), and a final covalent complex after proton transfer to the nitrile group (6). The distance (sulfur–carbon) of the catalytic Cys100 and the inhibitor’s C_{AB} atom is 3.2, 2.3, and 1.8 Å, respectively.

and 3c, respectively, and the transition state has lower “free” energy than the initial separated reactants (Table S6). The final covalent complexes with a S–C_{AB} separation of 1.8 Å are more stable by 9.2 and 5.4 kcal mol⁻¹ for 3a and 3c, respectively, compared to the noncovalent complexes, thus indicating that the “free” energy gain is higher for 3a also in the last step of the reaction (Table S6).

To conclude, the azanitrile 3a has more favorable thermodynamics of its reaction with SmCB1 by 10.2 kcal

mol⁻¹ compared to its carbanitrile analog (Table S6), which corresponds to their inhibitory potencies differing by several orders of magnitude (Table 1). The computational analysis showed that the carbanitrile inhibitor has the *Z*-configuration both in solution and in covalent complex with SmCB1, whereas the azanitrile inhibitor undergoes the *E*- to *Z*-transformation. Further, the *Z*-configuration of the azanitrile in the SmCB1 noncovalent complex is more stable than the *E*-configuration (by 3.5 kcal mol⁻¹, Supplementary Results),

Scheme 1. Synthesis of Compound 3c^a

^aReagents and conditions: (a) (1) $\text{ClCO}_2i\text{-Bu}$, NMM, THF, $-25\text{ }^\circ\text{C}$ and (2) $\text{H}_2\text{NCH}_2\text{CN} \times \text{H}_2\text{SO}_4$, NaOH, H_2O , THF, $-25\text{ }^\circ\text{C}$ to rt, 2 h; (b) TFA, CH_2Cl_2 , rt, 2 h; (c) benzyl isocyanate, Et_3N , CH_2Cl_2 , $0\text{ }^\circ\text{C}$ for 15 min to rt for 16 h.

suggesting that azanitrile binding involves a “configurational selection”⁴² determined by the topology of the SmCB1 active site. The linear dependence of the k_{obs} values on the inhibitor concentrations (Figure 2) indicates a one-step kinetic reaction mechanism of the slow-binding azanitrile inhibitor,⁴³ which is, however, composed of several distinct mechanistic events in the physicochemical reaction scheme. On the basis of computational analysis, *E*- to *Z*-conversion is the kinetic controlling step, while the covalent bond formation is not supposed to be attributed to the slow binding because the transition barrier TS_2 of azanitrile is even lower than that of the fast-binding carbanitrile. The slow binding observed for azanitriles is a known kinetic feature of several other chemotypes of covalent inhibitors of cysteine proteases.^{35,44–46}

CONCLUSIONS

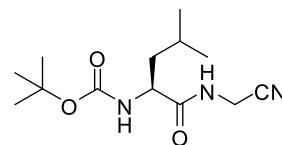
We investigated the inhibition potency of dipeptidomimetics with azanitrile and carbanitrile warheads against the cysteine protease SmCB1, a drug target from the human blood fluke *S. mansoni*. A screen of 68 compounds, including analog pairs of both chemotypes, demonstrated the nanomolar inhibition potency of the azanitriles and their general superior potency over their carbanitrile counterparts. Furthermore, the azanitriles were more quickly lethal to the schistosome parasite *in vitro* and, accordingly, represent a new class of compounds for the development of schistosomiasis drugs. The study provides a platform for further improvement of the azanitrile scaffold based on, for example, the introduction of a P3 triaryl moiety that is connected via an amide bond to a hydrophobic P2 amino acid and that proved particularly advantageous for SmCB1 inhibition. Further research will also address the selectivity of azanitrile inhibitors that are, in general, highly potent against human cysteine cathepsins with endopeptidase activity.^{6,7}

The atomic-level azanitrile–target interaction has not been elucidated up to now. In this study, we solved the first crystal structure of SmCB1 in complex with an azadipeptide nitrile and structurally analyzed the azanitrile-binding mode. By then analyzing the quantum chemical “free” energy profiles of the azanitrile- and carbanitrile-binding reactions with SmCB1, we demonstrated that the azanitriles alone undergo an *E*- to *Z*-conformational change upon binding to the enzyme, which we propose as an explanation for the different inhibition kinetic behavior of both chemotypes. Furthermore, azanitriles have a significantly higher “free” energy gain in three consecutive steps along the reaction coordinate, including formation of the initial noncovalent inhibitor–enzyme complex, the transition state, and the final covalent complex with the inhibitor warhead linked to the enzyme catalytic site. The data on the distinct conformational dynamics and binding energetics of the azanitrile warhead provide a mechanistic insight into the reactivity of azanitrile peptidomimetics.

METHODS

Synthesis of Inhibitors. General Conditions. Except for compound 3c, the inhibitors used in this study have been synthesized as described.^{6–8,47} Thin-layer chromatography was carried out on Merck (Darmstadt, Germany) aluminum sheets, silica gel 60 F254. Detection was performed with a UV light at 254 nm. Preparative column chromatography was performed on Merck silica gel (0.063–0.200 mm, 60 Å). Melting points were determined on a Büchi (Essen, Germany) 510 oil bath apparatus. ^1H NMR (500 MHz) and ^{13}C NMR (125 MHz) spectra were recorded on a Bruker Avance DRX 500 spectrometer and ^1H NMR (600 MHz) and ^{13}C NMR (150 MHz) spectra, on a Bruker Avance III 600 NMR spectrometer. Chemical shifts δ are given in ppm referring to the signal center using the solvent peaks for reference: $\text{DMSO-}d_6$ 2.49/39.7 ppm. LC-MS analyses were carried out on an API2000 (Applied Biosystems, Darmstadt, Germany) mass spectrometer coupled to an Agilent (Santa Clara, CA, USA) 1100 LC system using a Phenomenex Luna C18 column (Phenomenex, Aschaffenburg, Germany; 50×2.0 mm, particle size $3\ \mu\text{m}$). The purity of the compounds was determined using the diode array detector (DAD) of the LC-MS instrument on 196 and 400 nm. HRMS spectra were recorded on a microTOF-Q (Bruker, Köln, Germany) mass spectrometer connected to a Dionex (Thermo Scientific, Braunschweig, Germany) Ultimate 3000 LC via an ESI interface using a Nucleodur C18 Gravity column (50×2.0 mm I.D., $3\ \mu\text{m}$, Macherey-Nagel, Düren, Germany). The compounds were of at least 95% purity. All compounds passed the PAINS filter using a false positive remover.⁴⁸

(*S*)-*tert*-Butyl 1-(Cyanomethylamino)-4-methyl-1-oxopentan-2-ylcarbamate (II).

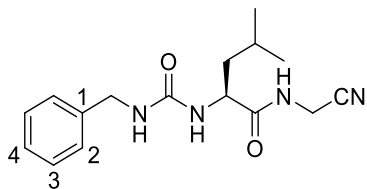


(*S*)-2-(*tert*-Butoxycarbonylamino)-4-methylpentanoic acid hydrate (I, 5.39 g, 21.6 mmol) was dissolved in anhydrous THF (30 mL) and cooled to $-25\text{ }^\circ\text{C}$. *N*-Methylmorpholine (2.61 mL, 2.41 g, 23.8 mmol) and isobutyl chloroformate (3.10 mL, 3.25 g, 23.8 mmol) were consecutively added to the stirred solution. Aminoacetonitrile monosulfate (6.65 g, 43.1 mmol) was suspended in H_2O (3 mL). The resulting suspension was treated with 5 N NaOH (17.0 mL) under ice-cooling and added to the reaction mixture when the precipitation of *N*-methylmorpholine hydrochloride occurred. It was allowed to warm to room temperature within 0.5 h and stirred for a further 1.5 h. After evaporation of the solvent, the resulting aqueous residue was extracted with EtOAc (3×30 mL). The combined organic layer was washed with aq. 10% KHSO_4 (30

mL), H₂O (30 mL), a sat. aq. NaHCO₃ solution (30 mL), H₂O (30 mL), and brine (30 mL). The solvent was dried over Na₂SO₄, filtered, and evaporated to dryness. The crude residue was purified by recrystallization from EtOAc/*n*-hexane to obtain **II** as a white solid (4.01 g, 69%); mp 118–120 °C (lit.⁴⁹ mp 114–116 °C) (Scheme 1).

¹H NMR (600 MHz, DMSO-*d*₆) δ 0.83 (d, ³J = 6.5 Hz, 3H) and 0.86 (d, ³J = 6.6 Hz, 3H, CH(CH₃)₂), 1.33–1.39 (m, 1H, CH–CHH), 1.36 (s, 9H, C(CH₃)₃), 1.43 (ddd, ²J = 13.6 Hz, ³J = 10.1 Hz, ³J = 5.2 Hz, 1H, CH–CHH), 1.52–1.63 (m, 1H, CH(CH₃)₂), 3.95 (td, ³J = 9.1 Hz, ³J = 4.8 Hz, 1H, NH–CH), 4.08–4.12 (m, 2H, CH₂–C≡N), 6.96 (d, ³J = 8.2 Hz, 1H, O–CO–NH), 8.52 (t, ³J = 5.7 Hz, 1H, CH–CO–NH). ¹³C NMR (150 MHz, DMSO-*d*₆) δ 21.56, 23.06 (CH(CH₃)₂), 24.41 (CH(CH₃)₂), 27.25 (NH–CH₂), 28.35 (C(CH₃)₃), 40.58 (CH–CH₂), 52.65 (NH–CH), 78.27 (C(CH₃)₃), 117.74 (C≡N), 155.55 (O–CO–NH), 173.49 (CH–CO–NH). LC-MS (ESI) (90% H₂O to 100% MeOH in 10 min, then 100% MeOH for 10 min, DAD 196–200 nm), 100% purity, *m/z* = 270.0 ([M + H]⁺), 287.0 ([M + NH₄]⁺).

(*S*)-2-(3-Benzylureido)-*N*-(cyanomethyl)-4-methylpentanamide (**3c**).



(*S*)-*tert*-Butyl 1-(cyanomethylamino)-4-methyl-1-oxopentan-2-ylcarbamate (**II**, 2.02 g, 7.50 mmol) was dissolved in anhydrous CH₂Cl₂ (200 mL) and treated with TFA (50 mL). The reaction mixture was stirred at room temperature for 2 h. The solvent was then evaporated, and the residue was diluted with CH₂Cl₂ (4 × 50 mL) and evaporated to remove the excess TFA. The crude product was dissolved in anhydrous CH₂Cl₂ (30 mL) and cooled to 0 °C. Subsequently, benzyl isocyanate (2.01 mL, 2.18 g, 16.3 mmol) was added, followed by triethylamine (5.15 mL, 3.76 g, 37.1 mmol). Stirring at 0 °C was prolonged for 15 min, and it then continued at room temperature overnight. After evaporation of the solvent, the residue was suspended in H₂O (50 mL) and extracted with EtOAc (3 × 75 mL). The organic layer was washed with aq. 10% KHSO₄ (50 mL), H₂O (50 mL), a sat. aq. NaHCO₃ solution (50 mL), H₂O (50 mL), and brine (50 mL), dried over Na₂SO₄, filtered, and evaporated to dryness. The crude residue was purified by preparative column chromatography using a gradient of petroleum ether/EtOAc (1:1) to EtOAc (100%), followed by recrystallization from EtOAc of the product containing fractions to give a white solid (0.34 g, 15%); mp 192–193 °C (Scheme 1).

¹H NMR (500 MHz, DMSO-*d*₆) δ 0.85 (d, ³J = 6.6 Hz, 3H) and 0.88 (d, ³J = 6.7 Hz, 3H, CH(CH₃)₂), 1.33–1.45 (m, 2H, CH–CH₂), 1.53–1.63 (m, 1H, CH(CH₃)₂), 4.07–4.11 (m, 2H, CH₂–C≡N), 4.18–4.22 (m, 2H, CH₂–NH–CO–NH), 6.17 (d, ³J = 8.4 Hz, 1H, NH–CH), 6.42 (t, ³J = 6.0 Hz, 1H, CH₂–NH–CO–NH), 7.17–7.25 (m, 3H, 2H, 4H), 7.26–7.33 (m, 2H, 3H), 8.66 (t, ³J = 5.6 Hz, 1H, CH–CO–NH). ¹³C NMR (125 MHz, DMSO-*d*₆) δ 21.96, 23.09 (CH(CH₃)₂), 24.42 (CH(CH₃)₂), 27.19 (NH–CH₂), 41.91 (CH–CH₂), 43.06 (CH₂–NH–CO–NH), 51.59 (CH–CH₂), 117.73 (C≡N), 126.77 (C-4), 127.13 (C-2), 128.39 (C-3), 140.75 (C-1),

157.76 (NH–CO–NH), 174.07 (CH–CO–NH). LC-MS (ESI) (90% H₂O to 100% MeOH in 10 min, then 100% MeOH for 10 min, DAD 210–400 nm), 99% purity, *m/z* = 302.9 ([M + H]⁺). HRMS, calcd. for C₁₆H₂₂N₄O₂: [M + H]⁺ *m/z* 303.1814; found: 303.1816.

Production of Recombinant SmCB1. A nonglycosylated mutant of the SmCB1 zymogen (Uniprot accession Q8MNY2) was expressed using the pPICZαA vector in the yeast *Pichia pastoris*, activated by *S. mansoni* legumain and purified as described previously.^{27,50} All purification steps were performed under reducing conditions in the presence of 2 mM dithiothreitol and 1 mM EDTA under an argon atmosphere to prevent the active site cysteine residue from oxidation.

Preparation of the SmCB1–Inhibitor Complex. The freshly activated SmCB1 (0.5 mg mL⁻¹) was incubated with a 4-fold molar excess of the inhibitor **3a** in 10 mM sodium acetate, pH 5.5, containing 20 mM cysteine and 1 mM EDTA, for 3 h at room temperature under an argon atmosphere. The enzyme inhibition was monitored using a kinetic assay with the fluorogenic substrate Cbz-Phe-Arg-AMC.²⁰ The complex was buffer-exchanged into 5 mM sodium acetate, pH 5.5, and concentrated to the final concentration of 4 mg mL⁻¹ using Amicon Ultracel-10k centrifugal units (Millipore, Burlington, USA); the inhibitor **3a** was maintained in a 4-fold molar excess to SmCB1 in the mixture.

Protein Crystallization and Data Collection. Crystals of the SmCB1–**3a** complex were obtained by vapor diffusion in a hanging drop. The drop consisting of 1 μL of protein solution and 1 μL of reservoir solution was equilibrated over 1 mL of reservoir solution at 20 °C. The reservoir solution contained 180 mM ammonium acetate, 80 mM sodium citrate, and 27% PEG 1500, pH 6.1. The protein concentration of the stock solution of the complex was 4 mg mL⁻¹ (in 5 mM sodium acetate, pH 5.5). The obtained needle-shaped crystal was flash-cooled by plunging into liquid nitrogen without cryoprotection. Diffraction data were collected at 100 K on the beamline MX14.1 operated by the Helmholtz-Zentrum Berlin at the BESSY II electron storage ring (Berlin-Adlershof, Germany).⁵¹ Diffraction data were processed using the XDS suite of programs.⁵² Crystal parameters and data collection statistics are given in Table S5.

Crystal Structure Determination. The SmCB1–**3a** complex crystallized in the orthorhombic space group P2₁2₁2₁ containing one molecule in the asymmetric unit and a solvent content of ~41% (Table S5). The structure of the SmCB1–**3a** complex was determined by molecular replacement with the program Molrep⁵³ from the CCP4 package⁵⁴ using the structure of the mature SmCB1 (PDB code: 3S3Q)²⁰ as the search model. Model refinement was carried out using the program REFMAC 5.2 from the CCP4 package,⁵⁴ interspersed with manual adjustments using Coot.⁵⁵ The structure was refined using data to a resolution of 1.3 Å. The final crystallographic model contains residues 70–323 (the SmCB1 zymogen numbering is used throughout the paper). Anisotropic refinement of all atomic displacement parameters (ADPs; B-factors) was included in the refinement protocol. The geometric restraints for ligand **3a** were constructed by the program Libcheck⁵⁴ using **3a** optimized by the DFT-D3/B3LYP/DZVP method combined with the COSMO⁵⁶ implicit solvent model. The optimization was performed by the Turbomole7.0⁵⁷ and Cuby4⁵⁸ programs. The **3a** molecule was modeled with an occupancy factor of 1 into generally well-defined electron density. The final refinement statistics are

given in Table S5. The quality of the final model was validated with Molprobit.⁵⁹ Atomic coordinates and structure factors have been deposited in the Protein Data Bank with the accession code 6YI7. The structure was analyzed using the program CONTACT.⁵⁴ All figures showing structural presentations were prepared with the program PyMOL 1.4 (Schrödinger, New York, USA).

Inhibition Assays. Inhibition measurements were performed in triplicates in 96-well microplates (100 μL assay volume) at 37 °C. SmCB1 (20–40 pM) was added to a mixture of the fluorogenic substrate Cbz-Phe-Arg-AMC (20 μM) and an inhibitor (0–100 μM) in 0.1 M sodium acetate, pH 5.5, containing 2.5 mM dithiothreitol and 0.1% PEG 6000. The substrate hydrolysis was monitored in an Infinite M1000 microplate reader (Tecan, Männedorf, Switzerland) at excitation and emission wavelengths of 360 and 465 nm, respectively, for up to 15 and 60 min for fast- and slow-binding inhibitors, respectively. Fast-binding inhibitors showed linear progress curves, and the apparent inhibition constant K_i' was determined by nonlinear regression using the equation $v_s/v_0 = 1/(1 + [I]/K_i')$ by the GraFit software (Erithacus Software, East Grinstead, UK), where v_s is the steady-state velocity, v_0 is the velocity in the absence of an inhibitor, and $[I]$ is the inhibitor concentration. For slow-binding inhibitors, an observed first-order rate constant k_{obs} was calculated at each inhibitor concentration by fitting the progress curve to the equation $P = v_s t + (v_i - v_s)(1 - \exp(k_{\text{obs}} t))/k_{\text{obs}} + d$, where P is the product formation, v_s is the steady-state velocity, t is the reaction time, v_i is the initial velocity, and d is the offset. The inhibition constant K_i' was determined by nonlinear regression using the equation $v_s/v_0 = 1/(1 + [I]/K_i')$. The true inhibition constants K_i were then calculated using the equation $K_i = K_i'/(1 + [S]/K_m)$, where $[S]$ is the substrate concentration and K_m is the Michaelis constant. The apparent second-order rate constant $k_{2\text{nd}}'$ was determined by fitting to the linear equation $k_{\text{obs}} = k_{2\text{nd}}'[I] + k_{\text{off}}$, where k_{off} is the first-order rate constants for the dissociation of the enzyme–inhibitor complex and the true constant $k_{2\text{nd}}$ was calculated by the correction $k_{2\text{nd}} = k_{2\text{nd}}'(1 + [S]/K_m)$. The K_m value determined for Cbz-Phe-Arg-AMC and SmCB1 was 25 μM . In none of the assay systems did the final concentration of DMSO exceed 1.5%.

Interaction Energy Calculations. The crystal structure of SmCB1 in complex with 3a was used for molecular modeling. Hydrogen atoms were added to the protein by the Reduce and Leap programs in AMBER 14⁶⁰ and to the ligand using PyMOL 1.7.6. Aspartates, glutamates, lysines, arginines, and histidines were charged (except for the neutral His270 in covalent complexes). Hydrogen atoms were relaxed by annealing from 1000 to 0 K at the MM level in AMBER 14. The FF14SB force field was used for the protein while the GAFF force field was used for the ligand. The cooling runs were 4 ps long with a 1 fs step and Berendsen thermostat used. Fourteen crystallographic water molecules were considered for the modeled complex. The 3c ligand was built manually using the PyMOL 1.7.6.

The QM part comprised residues within 2.5 Å of 3a (i.e., 300 atoms). The QM part was treated at the DFT-D3/BLYP/TZVPP level for single-point energy calculations. For gradient optimizations, we used the DFT-D3/BLYP/DZVP level.⁶¹ The rest of the system was treated at the PM6-D3H4X level.^{62,63} The environment was described by the COSMO implicit solvent model.⁵⁶ The coupling between QM and SQM was done by Cuby4,⁵⁸ which calls Turbomole 7.0⁵⁷ and Mopac⁶⁴

for QM and SQM, respectively. Residues further than 6 Å of 3a in the crystal structure were frozen during the optimization.

To generate the noncovalent complexes of 3a and 3b with SmCB1, it was necessary to break the covalent bond between the inhibitor and the S_G atom of Cys100 and transfer the hydrogen atom of the C=N–H group of the inhibitor to His270.³⁵ The bond was broken by employing harmonic restraints and relaxed scans. The obtained noncovalent complexes were reoptimized without any restraint and scored using the standard QM-based scoring function.^{35,65,66} The relative “free” energy of the noncovalent complex was computed as a sum of gas phase interaction energy (ΔE_{int}), interaction desolvation free energy ($\Delta\Delta G_{\text{solv}}$), and the change of the conformational “free” energy of the ligand ($\Delta G'_{\text{conf}}$).^{35,65,66} The ligand structures were optimized in solution by the same methodology as the complex. The solvation free energy of the studied ligands was computed by the SMD/HF/6-31G* method⁶⁷ implemented in Gaussian09.⁶⁸

Life Cycle of *Schistosoma mansoni*. *S. mansoni* (NMRI strain) is routinely maintained in the CDIPD by cycling between *Biomphalaria glabrata* snails and Golden Syrian hamsters.^{26,69,70} Vertebrate animal use is supported under a protocol approved by UC San Diego’s Institutional Animal Care and Use Committee (IACUC). The protocol complies with United States federal regulations regarding the care and use of laboratory animals: Public Law 99-158, the Health Research Extension Act, and Public Law 99-198, the Animal Welfare Act, which is regulated by USDA, APHIS, CFR, Title 9, Parts 1, 2, and 3. Informed consent of all participating subjects was obtained.

Schistosome Phenotypic Assay. Newly transformed schistosomula (NTS) of *S. mansoni* were prepared by mechanically transforming infective larvae (cercariae) as described previously.^{70,71} NTS (200–300 parasites) were incubated in 200 μL of Basch Medium 169 containing 5% FBS, 100 U mL^{-1} penicillin, and 100 $\mu\text{g mL}^{-1}$ streptomycin at 5% CO_2 and 37 °C.^{70,72,73} Inhibitors were added at the final concentration of 10 μM ,^{20,69} and changes in phenotypes were observed every 24 h for up to 4 days. A constrained nomenclature of “descriptors” is used to record the multiple and dynamic changes in movement, shape, and translucence of which the schistosome parasite is capable (Table S3).⁷⁰ These descriptors are then converted into an ordinal “severity score” system from 0 (no effect) to 4 (maximum effect), which allows for the relative comparison of compound effects, as described.^{74,75} Images of NTS were captured using a Zeiss Axiovert 40 C inverted microscope (10 \times objective) and a Zeiss AxioCam MRc digital camera controlled by AxioVision 40 (v. 4.8.1.0) software.

■ ASSOCIATED CONTENT

Supporting Information

The Supporting Information is available free of charge at <https://pubs.acs.org/doi/10.1021/acsinfectdis.0c00644>.

Supplementary methods, results, and six tables: (S1) inhibition of SmCB1 by azadipeptide nitriles, (S2) inhibition of SmCB1 by carbadipeptide nitriles, (S3) antischistosomal activity of azanitrile and carbanitrile inhibitors, (S4) cytotoxicity of the most potent azanitrile inhibitors of SmCB1, (S5) X-ray data collection and refinement statistics, and (S6) energy calculation of the

binding reaction of the inhibitors **3a** and **3c** to SmCB1; four figures: (S1) atom labeling scheme for the inhibitor **3a**, (S2) electron density maps for the inhibitor **3a**, (S3) energy calculation of the conformation change of the inhibitors **3a** and **3c**, and (S4) the molecular surface of the electrostatic potential (ESP) of the inhibitors **3a** and **3c** (PDF)

Accession Codes

Atomic coordinates and experimental structure factors for the SmCB1–**3a** complex have been deposited in the Protein Data Bank with accession code 6YI7.

AUTHOR INFORMATION

Corresponding Authors

Michael Mareš – Institute of Organic Chemistry and Biochemistry of the Czech Academy of Sciences, 16610 Prague 6, Czech Republic; Email: mares@uochb.cas.cz

Michael Gütschow – Pharmaceutical Institute, Pharmaceutical & Medicinal Chemistry, University of Bonn, 53121 Bonn, Germany; orcid.org/0000-0002-9376-7897; Email: guetschow@uni-bonn.de

Authors

Adéla Jílková – Institute of Organic Chemistry and Biochemistry of the Czech Academy of Sciences, 16610 Prague 6, Czech Republic; orcid.org/0000-0002-0847-5022

Martin Horn – Institute of Organic Chemistry and Biochemistry of the Czech Academy of Sciences, 16610 Prague 6, Czech Republic; orcid.org/0000-0001-9110-2018

Jindřich Fanfrlík – Institute of Organic Chemistry and Biochemistry of the Czech Academy of Sciences, 16610 Prague 6, Czech Republic

Jim Küppers – Pharmaceutical Institute, Pharmaceutical & Medicinal Chemistry, University of Bonn, 53121 Bonn, Germany

Petr Pachl – Institute of Organic Chemistry and Biochemistry of the Czech Academy of Sciences, 16610 Prague 6, Czech Republic

Pavlna Rezáčová – Institute of Organic Chemistry and Biochemistry of the Czech Academy of Sciences, 16610 Prague 6, Czech Republic

Martin Lepšík – Institute of Organic Chemistry and Biochemistry of the Czech Academy of Sciences, 16610 Prague 6, Czech Republic; orcid.org/0000-0003-2607-8132

Pavla Fajtová – Institute of Organic Chemistry and Biochemistry of the Czech Academy of Sciences, 16610 Prague 6, Czech Republic

Petra Rubešová – Institute of Organic Chemistry and Biochemistry of the Czech Academy of Sciences, 16610 Prague 6, Czech Republic

Marta Chanová – Institute of Immunology and Microbiology, First Faculty of Medicine, Charles University and General University Hospital in Prague, 12800 Prague 2, Czech Republic

Conor R. Caffrey – Center for Discovery and Innovation in Parasitic Diseases (CDIPD), Skaggs School of Pharmacy and Pharmaceutical Sciences, University of California San Diego, La Jolla, California 92093, United States

Complete contact information is available at:

<https://pubs.acs.org/10.1021/acsinfecdis.0c00644>

Author Contributions

[‡]A.J. and M.H. contributed equally to this work.

Notes

The authors declare no competing financial interest.

ACKNOWLEDGMENTS

The authors thank Brian M. Suzuki, Jiří Brynda, and Vojtěch Spiwok for technical assistance with the phenotypic assays involving the schistosome parasite, the crystallography, and the statistics analysis, respectively. We also thank Helena Mertlíková-Kaiserová for cytotoxicity data. This work was supported by grant LTAUSA19109 from the Ministry of Education, Youth and Sports of the Czech Republic (MEYS), grant NV18-05-00345 from the Ministry of Health of the Czech Republic, project ChemBioDrug CZ.02.1.01/0.0/0.0/16_019/0000729 from ERDF/OPRDE, Gilead Sciences & IOCB Research Center, and institutional projects RVO 61388963 and PROGRES Q25. J.F. and M.L. were supported by project LM2015070 from MEYS. Phenotypic screening at the CDIPD was supported in part by R21AI126296 from NIH-NIAID and OPP1171488 from the Bill and Melinda Gates Foundation. Diffraction data were collected on MX14.1 at the BESSY II electron storage ring operated by the Helmholtz-Zentrum Berlin.

ABBREVIATIONS

AMC, aminomethylcoumarin; Bn, benzyl; Cbz, benzyloxycarbonyl; Cha, cyclohexylalanine; Hph, homophenylalanine; NTS, newly transformed schistosomula; RMSD, root-mean-square deviation; SmCB1, cathepsin B1 from *Schistosoma mansoni*

REFERENCES

- (1) Chingle, R., Proulx, C., and Lubell, W. D. (2017) Azapeptide Synthesis Methods for Expanding Side-Chain Diversity for Biomedical Applications. *Acc. Chem. Res.* 50 (7), 1541–1556.
- (2) Proulx, C., Sabatino, D., Hopewell, R., Spiegel, J., Garcia Ramos, Y., and Lubell, W. D. (2011) Azapeptides and their therapeutic potential. *Future Med. Chem.* 3 (9), 1139–64.
- (3) Verhelst, S. H., Witte, M. D., Arastu-Kapur, S., Fonovic, M., and Bogyo, M. (2006) Novel aza peptide inhibitors and active-site probes of papain-family cysteine proteases. *ChemBioChem* 7 (6), 943–950.
- (4) Mir, F. M., Atmuri, N. D. P., Bourguet, C. B., Fores, J. R., Hou, X., Chemtob, S., and Lubell, W. D. (2019) Paired Utility of Aza-Amino Acyl Proline and Indolizidinone Amino Acid Residues for Peptide Mimicry: Conception of Prostaglandin F2alpha Receptor Allosteric Modulators That Delay Preterm Birth. *J. Med. Chem.* 62 (9), 4500–4525.
- (5) Sexton, K. B., Kato, D., Berger, A. B., Fonovic, M., Verhelst, S. H., and Bogyo, M. (2007) Specificity of aza-peptide electrophile activity-based probes of caspases. *Cell Death Differ.* 14 (4), 727–32.
- (6) Löser, R., Frizler, M., Schilling, K., and Gütschow, M. (2008) Azadipeptide nitriles: highly potent and proteolytically stable inhibitors of papain-like cysteine proteases. *Angew. Chem., Int. Ed.* 47 (23), 4331–4334.
- (7) Frizler, M., Lohr, F., Furtmann, N., Kläs, J., and Gütschow, M. (2011) Structural optimization of azadipeptide nitriles strongly increases association rates and allows the development of selective cathepsin inhibitors. *J. Med. Chem.* 54 (1), 396–400.
- (8) Frizler, M., Lohr, F., Lülsdorff, M., and Gütschow, M. (2011) Facing the gem-dialkyl effect in enzyme inhibitor design: preparation of homocycloleucine-based azadipeptide nitriles. *Chem. - Eur. J.* 17 (41), 11419–23.

- (9) Frizler, M., Schmitz, J., Schulz-Fincke, A. C., and Gütschow, M. (2012) Selective nitrile inhibitors to modulate the proteolytic synergism of cathepsins S and F. *J. Med. Chem.* 55 (12), 5982–6.
- (10) Yang, P. Y., Wang, M., Li, L., Wu, H., He, C. Y., and Yao, S. Q. (2012) Design, synthesis and biological evaluation of potent azadipeptide nitrile inhibitors and activity-based probes as promising anti-*Trypanosoma brucei* agents. *Chem. - Eur. J.* 18 (21), 6528–41.
- (11) Loh, Y., Shi, H., Hu, M., and Yao, S. Q. (2010) Click[®] synthesis of small molecule-peptide conjugates for organelle-specific delivery and inhibition of lysosomal cysteine proteases. *Chem. Commun. (Cambridge, U. K.)* 46 (44), 8407–9.
- (12) Löser, R., Bergmann, R., Frizler, M., Mosch, B., Dombrowski, L., Kuchar, M., Steinbach, J., Gütschow, M., and Pietzsch, J. (2013) Synthesis and radiopharmacological characterisation of a fluorine-18-labelled azadipeptide nitrile as a potential PET tracer for *in vivo* imaging of cysteine cathepsins. *ChemMedChem* 8 (8), 1330–44.
- (13) Van Kersavond, T., Nguyen, M. T. N., and Verhelst, S. H. L. (2017) Synthesis and Application of Activity-Based Probes for Proteases. *Methods Mol. Biol.* 1574, 255–266.
- (14) Tan, M. S. Y., Davison, D., Sanchez, M. I., Anderson, B. M., Howell, S., Snijders, A., Edgington-Mitchell, L. E., and Deu, E. (2020) Novel broad-spectrum activity-based probes to profile malarial cysteine proteases. *PLoS One* 15 (1), No. e0227341.
- (15) Deu, E. (2017) Proteases as antimalarial targets: strategies for genetic, chemical, and therapeutic validation. *FEBS J.* 284 (16), 2604–2628.
- (16) Boudreau, P. D., Miller, B. W., McCall, L. I., Almaliti, J., Reher, R., Hirata, K., Le, T., Siqueira-Neto, J. L., Hook, V., and Gerwick, W. H. (2019) Design of Gallinamide A Analogs as Potent Inhibitors of the Cysteine Proteases Human Cathepsin L and *Trypanosoma cruzi* Cruzain. *J. Med. Chem.* 62 (20), 9026–9044.
- (17) Ettari, R., Previti, S., Maiorana, S., Amendola, G., Wagner, A., Cosconati, S., Schirmeister, T., Hellmich, U. A., and Zappala, M. (2019) Optimization Strategy of Novel Peptide-Based Michael Acceptors for the Treatment of Human African Trypanosomiasis. *J. Med. Chem.* 62 (23), 10617–10629.
- (18) Ettari, R., Previti, S., Di Chio, C., and Zappala, M. (2020) Falcipain-2 and falcipain-3 inhibitors as promising antimalarial agents. *Curr. Med. Chem.*, DOI: 10.2174/0929867327666200730215316.
- (19) Sajid, M., McKerrow, J. H., Hansell, E., Mathieu, M. A., Lucas, K. D., Hsieh, I., Greenbaum, D., Bogyo, M., Salter, J. P., Lim, K. C., Franklin, C., Kim, J. H., and Caffrey, C. R. (2003) Functional expression and characterization of *Schistosoma mansoni* cathepsin B and its trans-activation by an endogenous asparaginyl endopeptidase. *Mol. Biochem. Parasitol.* 131 (1), 65–75.
- (20) Jílková, A., Řezáčová, P., Lepšík, M., Horn, M., Váchová, J., Fanfrlík, J., Brynda, J., McKerrow, J. H., Caffrey, C. R., and Mareš, M. (2011) Structural Basis for Inhibition of Cathepsin B Drug Target from the Human Blood Fluke, *Schistosoma mansoni*. *J. Biol. Chem.* 286 (41), 35770–35781.
- (21) Colley, D. G., Bustinduy, A. L., Secor, W. E., and King, C. H. (2014) Human schistosomiasis. *Lancet* 383 (9936), 2253–2264.
- (22) Caffrey, C. R. (2007) Chemotherapy of schistosomiasis: present and future. *Curr. Opin. Chem. Biol.* 11 (4), 433–439.
- (23) Caffrey, C. R., and Secor, W. E. (2011) Schistosomiasis: from drug deployment to drug development. *Curr. Opin. Infect. Dis.* 24 (5), 410–417.
- (24) Thetiot-Laurent, S. A., Boissier, J., Robert, A., and Meunier, B. (2013) Schistosomiasis chemotherapy. *Angew. Chem., Int. Ed.* 52 (31), 7936–7956.
- (25) Caffrey, C. R., El-Sakkary, N., Mäder, P., Krieg, R., Becker, K., Schlitzer, M., Drewry, D. H., Vennerstrom, J. L., and Grevelding, C. G. (2019) Drug Discovery and Development for Schistosomiasis. In *Neglected Tropical Diseases* (Swinney, D., Pollastri, M., Mannhold, R., Buschmann, H., and Holenz, J., Eds.), Wiley, Weinheim, Germany.
- (26) Abdulla, M. H., Lim, K. C., Sajid, M., McKerrow, J. H., and Caffrey, C. R. (2007) Schistosomiasis mansoni: novel chemotherapy using a cysteine protease inhibitor. *PLoS Med.* 4 (1), No. e14.
- (27) Horn, M., Jílková, A., Vondrášek, J., Marešová, L., Caffrey, C. R., and Mareš, M. (2011) Mapping the Pro-Peptide of the *Schistosoma mansoni* Cathepsin B1 Drug Target: Modulation of Inhibition by Heparin and Design of Mimetic Inhibitors. *ACS Chem. Biol.* 6 (6), 609–617.
- (28) Jílková, A., Horn, M., Řezáčová, P., Marešová, L., Fajtova, P., Brynda, J., Vondrášek, J., McKerrow, J. H., Caffrey, C. R., and Mareš, M. (2014) Activation Route of the *Schistosoma mansoni* Cathepsin B1 Drug Target: Structural Map with a Glycosaminoglycan Switch. *Structure* 22 (12), 1786–1798.
- (29) Schechter, I., and Berger, A. (1967) On the size of the active site in proteases. I. Papain. *Biochem. Biophys. Res. Commun.* 27 (2), 157–62.
- (30) Thompson, S. A., Andrews, P. R., and Hanzlik, R. P. (1986) Carboxyl-modified amino acids and peptides as protease inhibitors. *J. Med. Chem.* 29 (1), 104–11.
- (31) Schmitz, J., Gilberg, E., Löser, R., Bajorath, J., Bartz, U., and Gütschow, M. (2019) Cathepsin B: Active site mapping with peptidic substrates and inhibitors. *Bioorg. Med. Chem.* 27 (1), 1–15.
- (32) Greenspan, P. D., Clark, K. L., Tommasi, R. A., Cowen, S. D., McQuire, L. W., Farley, D. L., van Duzer, J. H., Goldberg, R. L., Zhou, H., Du, Z., Fitt, J. J., Coppa, D. E., Fang, Z., Macchia, W., Zhu, L., Capparelli, M. P., Goldstein, R., Wigg, A. M., Doughty, J. R., Bohacek, R. S., and Knap, A. K. (2001) Identification of dipeptidyl nitriles as potent and selective inhibitors of cathepsin B through structure-based drug design. *J. Med. Chem.* 44 (26), 4524–4534.
- (33) Ottersbach, P. A., Schnakenburg, G., and Gütschow, M. (2012) Induction of chirality: experimental evidence of atropisomerism in azapeptides. *Chem. Commun. (Cambridge, U. K.)* 48 (46), 5772–4.
- (34) Ottersbach, P. A., Schmitz, J., Schnakenburg, G., and Gütschow, M. (2013) An access to aza-Freidinger lactams and E-locked analogs. *Org. Lett.* 15 (3), 448–51.
- (35) Fanfrlík, J., Brahmikshatriya, P. S., Řezáč, J., Jílková, A., Horn, M., Mareš, M., Hobza, P., and Lepšík, M. (2013) Quantum Mechanics-Based Scoring Rationalizes the Irreversible Inactivation of Parasitic *Schistosoma mansoni* Cysteine Peptidase by Vinyl Sulfone Inhibitors. *J. Phys. Chem. B* 117 (48), 14973–14982.
- (36) Mladenovic, M., Fink, R. F., Thiel, W., Schirmeister, T., and Engels, B. (2008) On the origin of the stabilization of the zwitterionic resting state of cysteine proteases: a theoretical study. *J. Am. Chem. Soc.* 130 (27), 8696–705.
- (37) Paasche, A., Schirmeister, T., and Engels, B. (2013) Benchmark Study for the Cysteine-Histidine Proton Transfer Reaction in a Protein Environment: Gas Phase, COSMO, QM/MM Approaches. *J. Chem. Theory Comput.* 9 (3), 1765–77.
- (38) Schirmeister, T., Kesselring, J., Jung, S., Schneider, T. H., Weickert, A., Becker, J., Lee, W., Bamberger, D., Wich, P. R., Distler, U., Tenzer, S., Johe, P., Hellmich, U. A., and Engels, B. (2016) Quantum Chemical-Based Protocol for the Rational Design of Covalent Inhibitors. *J. Am. Chem. Soc.* 138 (27), 8332–5.
- (39) Quesne, M. G., Ward, R. A., and de Visser, S. P. (2013) Cysteine protease inhibition by nitrile-based inhibitors: a computational study. *Front. Chem.* 1, 39.
- (40) Löser, R., Pitzschler, R., and Köckerling, M. (2017) Synthesis and X-ray Crystal Structure of N¹-Cyano-N,N¹-dimethyl-4-nitrobenzohydrazide. *Crystals* 7 (10), 290.
- (41) Licandro, E., and Perdicchia, D. (2004) N-acylhydrazines: Future perspectives offered by new syntheses and chemistry. *Eur. J. Org. Chem.* 2004 (4), 665–675.
- (42) Vogt, A. D., and Di Cera, E. (2012) Conformational selection or induced fit? A critical appraisal of the kinetic mechanism. *Biochemistry* 51 (30), 5894–902.
- (43) Copeland, R. A. (2013) Slow Binding Inhibitors. In *Evaluation of Enzyme Inhibitors in Drug Discovery: A Guide for Medicinal Chemists and Pharmacologists*, pp 203–244, John Wiley.
- (44) Miller, B., Friedman, A. J., Choi, H., Hogan, J., McCammon, J. A., Hook, V., and Gerwick, W. H. (2014) The marine cyanobacterial metabolite gallinamide A is a potent and selective inhibitor of human cathepsin L. *J. Nat. Prod.* 77 (1), 92–9.

- (45) Shokhen, M., Khazanov, N., and Albeck, A. (2011) The mechanism of papain inhibition by peptidyl aldehydes. *Proteins: Struct., Funct., Genet.* 79 (3), 975–85.
- (46) Brady, K. D. (1998) Bimodal inhibition of caspase-1 by aryloxymethyl and acyloxymethyl ketones. *Biochemistry* 37 (23), 8508–15.
- (47) Laube, M., Frizler, M., Wodtke, R., Neuber, C., Belter, B., Kniess, T., Bachmann, M., Gütschow, M., Pietzsch, J., and Löser, R. (2019) Synthesis and preliminary radiopharmacological characterisation of an ¹¹C-labelled azadipeptide nitrile as potential PET tracer for imaging of cysteine cathepsins. *J. Labelled Compd. Radiopharm.* 62 (8), 448–459.
- (48) Baell, J. B., and Holloway, G. A. (2010) New substructure filters for removal of pan assay interference compounds (PAINS) from screening libraries and for their exclusion in bioassays. *J. Med. Chem.* 53 (7), 2719–40.
- (49) Löser, R., Schilling, K., Dimmig, E., and Gütschow, M. (2005) Interaction of papain-like cysteine proteases with dipeptide-derived nitriles. *J. Med. Chem.* 48 (24), 7688–707.
- (50) Jílková, A., Horn, M., and Mareš, M. (2020) Structural and Functional Characterization of *Schistosoma mansoni* Cathepsin B1. *Methods Mol. Biol.* 2151, 145–158.
- (51) Mueller, U., Forster, R., Hellmig, M., Huschmann, F. U., Kastner, A., Malecki, P., Puhlinger, S., Rower, M., Sparta, K., Steffien, M., Uhlein, M., Wilk, P., and Weiss, M. S. (2015) The macromolecular crystallography beamlines at BESSY II of the Helmholtz-Zentrum Berlin: Current status and perspectives. *Eur. Phys. J. Plus* 130 (7), 141.
- (52) Kabsch, W. (2010) Xds. *Acta Crystallogr., Sect. D: Biol. Crystallogr.* 66 (2), 125–132.
- (53) Vagin, A., and Teplyakov, A. (2000) An approach to multi-copy search in molecular replacement. *Acta Crystallogr., Sect. D: Biol. Crystallogr.* 56 (12), 1622–1624.
- (54) Winn, M. D., Ballard, C. C., Cowtan, K. D., Dodson, E. J., Emsley, P., Evans, P. R., Keegan, R. M., Krissinel, E. B., Leslie, A. G., McCoy, A., McNicholas, S. J., Murshudov, G. N., Pannu, N. S., Potterton, E. A., Powell, H. R., Read, R. J., Vagin, A., and Wilson, K. S. (2011) Overview of the CCP4 suite and current developments. *Acta Crystallogr., Sect. D: Biol. Crystallogr.* 67 (4), 235–242.
- (55) Emsley, P., and Cowtan, K. (2004) Coot: model-building tools for molecular graphics. *Acta Crystallogr., Sect. D: Biol. Crystallogr.* 60 (12), 2126–2132.
- (56) Klamt, A., and Schuurmann, G. (1993) Cosmo - a New Approach to Dielectric Screening in Solvents with Explicit Expressions for the Screening Energy and Its Gradient. *J. Chem. Soc., Perkin Trans. 2* No. 5, 799–805.
- (57) Ahlrichs, R., Bar, M., Haser, M., Horn, H., and Kolmel, C. (1989) Electronic-Structure Calculations on Workstation Computers - the Program System Turbomole. *Chem. Phys. Lett.* 162 (3), 165–169.
- (58) Řezáč, J. (2016) Cuby: An integrative framework for computational chemistry. *J. Comput. Chem.* 37 (13), 1230–7.
- (59) Lovell, S. C., Davis, I. W., Arendall, W. B., III, de Bakker, P. I., Word, J. M., Prisant, M. G., Richardson, J. S., and Richardson, D. C. (2003) Structure validation by α geometry: φ , ψ and $C\beta$ deviation. *Proteins: Struct., Funct., Genet.* 50 (3), 437–450.
- (60) Case, D. A., Babin, V., Berryman, J. T., Betz, R. M., Cai, Q., Cerutti, D. S., Cheatham, T. E., Darden, T. A., Duke, R. E., Gohlke, H., Goetz, A. W., Gusarov, S., Homeyer, N., Janowski, P., Kaus, J., Kolossváry, I., Kovalenko, A., Lee, T. S., LeGrand, S., Luchko, T., Luo, R., Madej, B., Merz, K. M., Paesani, F., Roe, D. R., Roitberg, A., Sagui, C., Salomon-Ferrer, R., Sebabra, G., Simmerling, C. L., Smith, W., Swails, J., Walker, R. C., Wang, J., Wolf, R. M., Wu, X., and Kollman, P. A. (2014) *AMBER 14*, University of California San Francisco, San Francisco (USA).
- (61) Hostaš, J., and Řezáč, J. (2017) Accurate DFT-D3 Calculations in a Small Basis Set. *J. Chem. Theory Comput.* 13 (8), 3575–3585.
- (62) Stewart, J. J. (2007) Optimization of parameters for semiempirical methods V: modification of NDDO approximations and application to 70 elements. *J. Mol. Model.* 13 (12), 1173–213.
- (63) Řezáč, J., and Hobza, P. (2012) Advanced Corrections of Hydrogen Bonding and Dispersion for Semiempirical Quantum Mechanical Methods. *J. Chem. Theory Comput.* 8 (1), 141–51.
- (64) Stewart, J. J. P. (2004) Optimization of parameters for semiempirical methods IV: extension of MNDO, AM1, and PM3 to more main group elements. *J. Mol. Model.* 10 (2), 155–164.
- (65) Fanfrlík, J., Bronowska, A. K., Řezáč, J., Přenosil, O., Konvalinka, J., and Hobza, P. (2010) A reliable docking/scoring scheme based on the semiempirical quantum mechanical PM6-DH2 method accurately covering dispersion and H-bonding: HIV-1 protease with 22 ligands. *J. Phys. Chem. B* 114 (39), 12666–78.
- (66) Lepšík, M., Řezáč, J., Kolář, M., Pecina, A., Hobza, P., and Fanfrlík, J. (2013) The Semiempirical Quantum Mechanical Scoring Function for In Silico Drug Design. *ChemPlusChem* 78 (9), 921–931.
- (67) Marenich, A. V., Cramer, C. J., and Truhlar, D. G. (2009) Performance of SM6, SM8, and SMD on the SAMPL1 test set for the prediction of small-molecule solvation free energies. *J. Phys. Chem. B* 113 (14), 4538–43.
- (68) Frisch, M. J., Trucks, G. W., Schlegel, H. B., Scuseria, G. E., Robb, M. A., Cheeseman, J. R., Scalmani, G., Barone, V., Petersson, G. A., Nakatsuji, H., Li, X., Caricato, M., Marenich, A. V., Bloino, J., Janesko, B. G., Gomperts, R., Mennucci, B., Hratchian, H. P., Ortiz, J. V., Izmaylov, A. F., Sonnenberg, J. L., Williams Ding, F., Lipparini, F., Egidi, F., Goings, J., Peng, B., Petrone, A., Henderson, T., Ranasinghe, D., Zakrzewski, V. G., Gao, J., Rega, N., Zheng, G., Liang, W., Hada, M., Ehara, M., Toyota, K., Fukuda, R., Hasegawa, J., Ishida, M., Nakajima, T., Honda, Y., Kitao, O., Nakai, H., Vreven, T., Throssell, K., Montgomery, J. A., Jr., Peralta, J. E., Ogliaro, F., Bearpark, M. J., Heyd, J. J., Brothers, E. N., Kudin, K. N., Staroverov, V. N., Keith, T. A., Kobayashi, R., Normand, J., Raghavachari, K., Rendell, A. P., Burant, J. C., Iyengar, S. S., Tomasi, J., Cossi, M., Millam, J. M., Klene, M., Adamo, C., Cammi, R., Ochterski, J. W., Martin, R. L., Morokuma, K., Farkas, O., Foresman, J. B., and Fox, D. J. (2016) *Gaussian 16*, Rev. C.01, Gaussian, Inc., Wallingford (USA).
- (69) Fajtová, P., Štefanić, S., Hradilek, M., Dvořák, J., Vondrášek, J., Jílková, A., Ulrychová, L., McKerrow, J. H., Caffrey, C. R., Mareš, M., and Horn, M. (2015) Prolyl Oligopeptidase from the Blood Fluke *Schistosoma mansoni*: From Functional Analysis to Anti-schistosomal Inhibitors. *PLoS Neglected Trop. Dis.* 9 (6), No. e0003827.
- (70) Abdulla, M. H., Ruelas, D. S., Wolff, B., Snedecor, J., Lim, K. C., Xu, F., Renslo, A. R., Williams, J., McKerrow, J. H., and Caffrey, C. R. (2009) Drug discovery for schistosomiasis: hit and lead compounds identified in a library of known drugs by medium-throughput phenotypic screening. *PLoS Neglected Trop. Dis.* 3 (7), No. e478.
- (71) Štefanić, S., Dvořák, J., Horn, M., Braschi, S., Sojka, D., Ruelas, D. S., Suzuki, B., Lim, K.-C., Hopkins, S. D., McKerrow, J. H., and Caffrey, C. R. (2010) RNA Interference in *Schistosoma mansoni* Schistosomula: Selectivity, Sensitivity and Operation for Larger-Scale Screening. *PLoS Neglected Trop. Dis.* 4 (10), No. e850.
- (72) Leontovych, A., Ulrychová, L., Horn, M., and Dvořák, J. (2020) Collection of Excretory/Secretory Products from Individual Developmental Stages of the Blood Fluke *Schistosoma mansoni*. *Methods Mol. Biol.* 2151, 55–63.
- (73) Dvořák, J., Fajtová, P., Ulrychová, L., Leontovych, A., Rojo-Arreola, L., Suzuki, B. M., Horn, M., Mareš, M., Craik, C. S., Caffrey, C. R., and O'Donoghue, A. J. (2016) Excretion/secretion products from *Schistosoma mansoni* adults, eggs and schistosomula have unique peptidase specificity profiles. *Biochimie* 122, 99–109.
- (74) Glaser, J., Schurigt, U., Suzuki, B. M., Caffrey, C. R., and Holzgrabe, U. (2015) Anti-Schistosomal Activity of Cinnamic Acid Esters: Eugenyl and Thymyl Cinnamate Induce Cytoplasmic Vacuoles and Death in Schistosomula of *Schistosoma mansoni*. *Molecules* 20 (6), 10873–83.
- (75) Long, T., Neitz, R. J., Beasley, R., Kalyanaraman, C., Suzuki, B. M., Jacobson, M. P., Dissous, C., McKerrow, J. H., Drewry, D. H., Zuercher, W. J., Singh, R., and Caffrey, C. R. (2016) Structure-

Bioactivity Relationship for Benzimidazole Thiophene Inhibitors of Polo-Like Kinase 1 (PLK1), a Potential Drug Target in *Schistosoma mansoni*. *PLoS Neglected Trop. Dis.* 10 (1), No. e0004356.